Iraqi Geological Journal

Journal homepage: https://www.igj-iraq.org

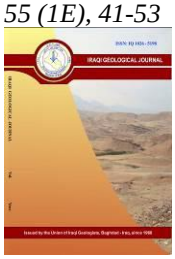

The Impact of Matrix Acidizing on the Petrophysical Properties of the Mishrif Formation: Experimental Investigation

Usama Alameedy[1,*] and Ayad A. Al-haleem[1]

[1] Petroleum Engineering Department, College of Engineering, University of Baghdad, Baghdad, Iraq

***** **Correspondence**: usama.sahib@coeng.uobaghdad.edu.iq

Received:
15 December 2021

Accepted:
21 March 2022

Published:
31 May 2022

Abstract

Matrix acidizing is a good stimulation process in which acid is introduced into the reservoir near the wellbore area via the wellbore or coil tubing. In the oil industry, formation damage is a prevalent problem. Bypassing wellbore damage by producing wormholes in carbonate reservoirs is the main purpose of acidizing the matrix of the formation. When doing lab tests, scientists are looking for a wormhole-inducing injection rate that can be used in the field. Meantime the ongoing works on the Ahdeb oil field's Mishrif reservoir, several reports have documented the difficulties encountered during stimulation operations, including high injection pressures that make it difficult to inject acid into the reservoir formation; and only a few acid jobs have been successful in Ahdeb oil wells, while the majority of the others have been failures; For this formation, there is a high incidence of oil well stimulation failed. This requires more study. Thus, in this work, we experimented to examine the effect of acid treatment on the petrophysical parameters of the Mishrif reservoir. The acid core-flood tests used seven core samples from a central Iraqi oil field.

Keywords: Mishrif reservoir; Matrix acidizing; Wormholes; Stimulation operations; Acid core-flood

1. Introduction

Since oil and gas exploration has relied on carbonate rocks for so much of its history, it is no surprise that around 40% of global reserves are found in these rocks (Jardine and Wilshart, 1982). Its chemical composition allows for successful acid injection stimulation despite variations in porosity and permeability depending on the location of the carbonate deposit. In both basic and practical terms, the chemical interaction and dissolving process between a fluid and the porous media through which it travels is of interest. The porous solid is carved with flow channels as the reactant dissolves the medium. Flow conditions and response rates influence the structure and behavior of dominating channels. An understanding of porous media channeling is required in order to forecast reaction zone or dissolution zone movement (Hoefner and Fogler, 1988).

The findings of this research may be used to improve the recovery of oil from the Mishrif reservoir. Known as "stimulating treatments," these techniques pour acid into wells in order to dissolve part of the porous rock surrounding the wellbore, increasing its permeability or flow capacity. Following stimulation, the channels created by dissolution allow for easier movement of oil out of the reservoir. By injecting acids into the wellbore, matrix acidizing has been routinely employed to increase well productivity. Acid spreads throughout the rock by forming wormholes, which are channels with high

DOI: 10.46717/igj.55.1E.4Ms-2022-05-20

permeability. Reducing the thickness of the skin around the wellbore increases throughput. According to acidizing recommendations by industry, hydrochloric acid (HCl) is the most often utilized acid for carbonate reservoir matrix acidization (McLeod, 1984). HCl is the acid of preference for acidizing techniques for most carbonate formations and is the base acid usually combined with other acids such as hydrofluoric (HF) in most sandstone applications (Alhamad et al., 2020). As an additional option, carbonates with extensive damage may be treated using acid systems based on HCl. The following is the chemical reaction that accounts for acid dissolution and carbonate formation:

$$CaCO_3 + 2HCl \rightarrow CaCl_2 + CO_2 + H_2O$$

The creation of wormholes in carbonate acidizing is essential to the stimulating effect. Both the acid's reactivity and the rate at which it is injected are critical to this process. In order to construct the most effective wormholes, it is necessary to manage the diffusion and reaction rates of HCl and carbonate. Interstitial velocity (vi) is often plotted against pore volume to determine how deep a wormhole may go in a wellbore. The deeper the wormhole goes, the deeper the wellbore is penetrated.

Matrix acidizing core flooding system was the initial target of this research process. Instructions for performing tests and troubleshooting solutions for apparatus were part of the second goal of the project. Acid transport and response speeds must be adjusted in order to optimize acidizing efficiency and maximize the stimulation's effect. This objective might be achieved by physical or chemical techniques. Various substances are used in the chemical reduction of reactivity in order to prevent a fast reaction from occurring. High-resolution images of three acidized Indiana limestone core samples from the (McDuff et al., 2010) investigation are displayed in Fig. 1. For Indiana limestone, the core plugs were chosen in accordance with the wormhole efficiency curve at various acid flow levels, from the lowest to the highest.

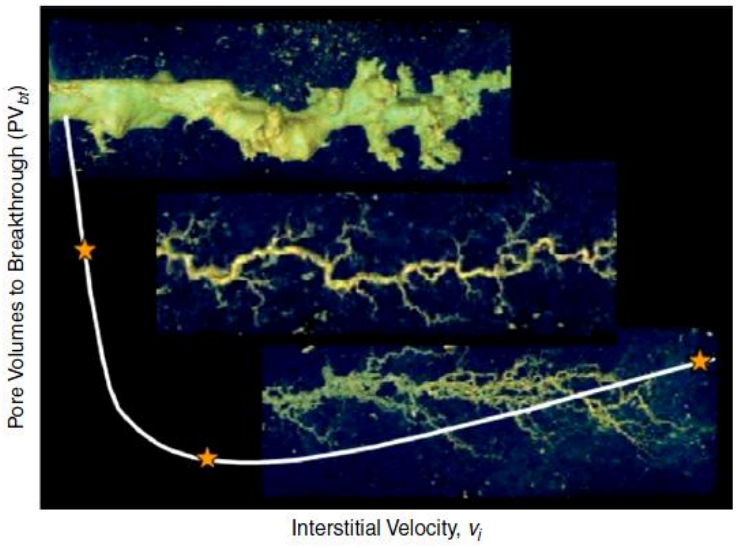

Fig.1. Three core samples of high-resolution CT scans (McDuff et al., 2010)

Acidification has been studied mathematically using a variety of models, including the dimensionless model, the capillary tube model, the network model, and the continuum model (Schecter and Gidley, 1969; Hung, Hill and Sepehrnoori, 1989; Fredd and Fogler, 1996; Gdanski, 1999; Maheshwari and Balakotaiah, 2013). Acidization and dissolution patterns, as determined by 1-D and 2-D numerical simulations, as well as experimental research by (Bazin, Charbonnel and Onaisi, 1999), are illustrated in Fig. 2 in a qualitative comparison. According to this Figure, 1-D numerical simulations anticipate greater optimal acid injection rates and larger pores to breakthrough (PVBT) than 3-D numerical simulations. A variety of disintegration patterns cannot be predicted using 1-D numerical simulations (such as conical, wormhole and ramified). The transport and reaction factors impacting

dissolution may be gleaned through 1-D numerical simulations, which are computationally cheap. Some of the dissolution patterns seen in the laboratory may be anticipated using 2-D computational models; however, these models cannot predict the optimal injection rate and PVBT.

Consequently, in order to accurately forecast the experimental outcomes, we will need to use 3-D numerical simulations. It's been a while since any 3-D numerical studies have been done to understand better the dissolving process (Cohen et al., 2008; de Oliveira et al., 2012; Ratnakar, Kalia and Balakotaiah, 2012). HCl, on the other hand, is a fast-acting acid, and these studies may not be able to accurately anticipate its findings.

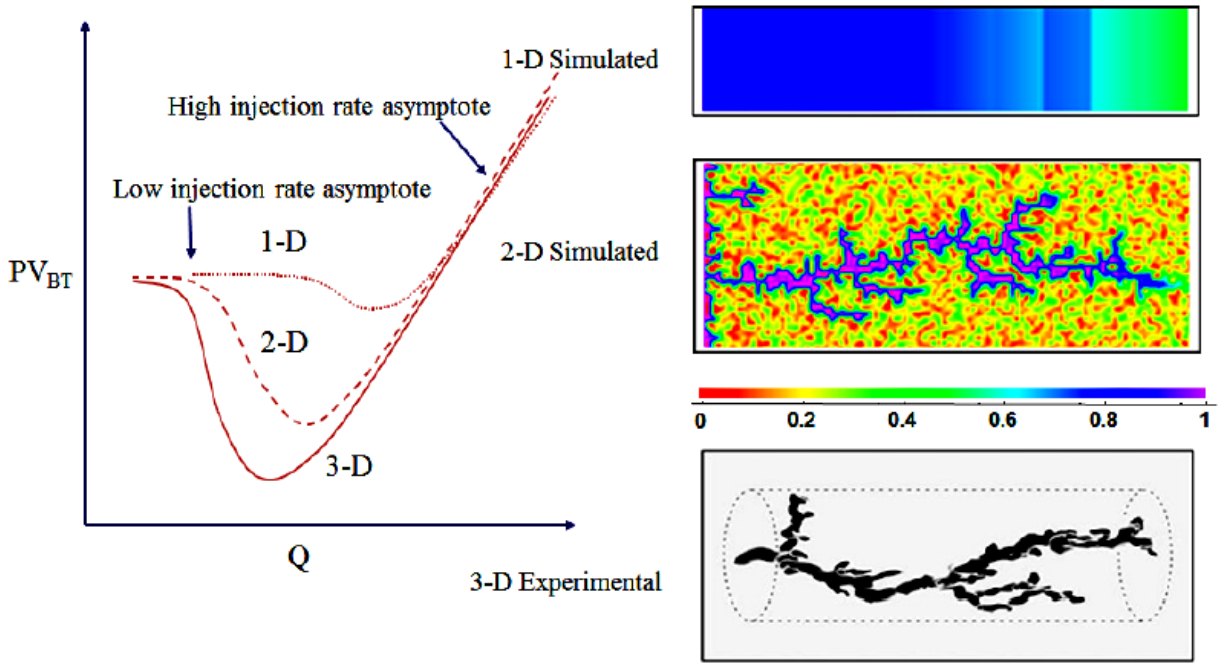

Fig.2. Dissolution patterns generated by 1-D, 2-D numerical simulations and experimental research by (Bazin, 2001) were compared to acidization curves (Panga, Balakotaiah and Ziauddin, 2002)

McDuff et al. (2010) used high-end numerical simulation models created from the 3-D digital representation of a well's whole 3-D shape to explore how wormhole changes occur over time. An advanced gridding method is used to mesh both the near-well rock matrix and the void space inside the wormholes. Fig. 3 illustrates how multi-phase flow simulations may be carried out.

2. Materials and Methods

2.1. Geological and Petrophysical Properties of Mishrif Reservoir

The thin section photomicrographs of the cored sections of Mishrif reservoir's well AD-12 used for this study are shown in Fig. 4. A total of seven (7) rock samples were used in this study: samples 1 – 4 were extracted from section A (composed mainly of echinoderm green algae micrite limestone), while samples 5 – 7 were cored from section B (micrite orbitolina sand grain limestone). The lithology comprises a wide range of limestone. The lithology on the bottom does not show light grey limestone separated with oil revealing light grey limestone underneath Rumaila. Both sets are composed mainly of calcite mineral and 1 – 1.5% clay content. The filling material is micrite. There are 34 zones interpreted in this well. An aggregate of 135.8m is accumulated with the overall thickness of the 19 oil and poor oil

zones. The entire thickness is 57.2m, with seven transition zones. There are 8 water zones with an overall thickness of 150.8m.

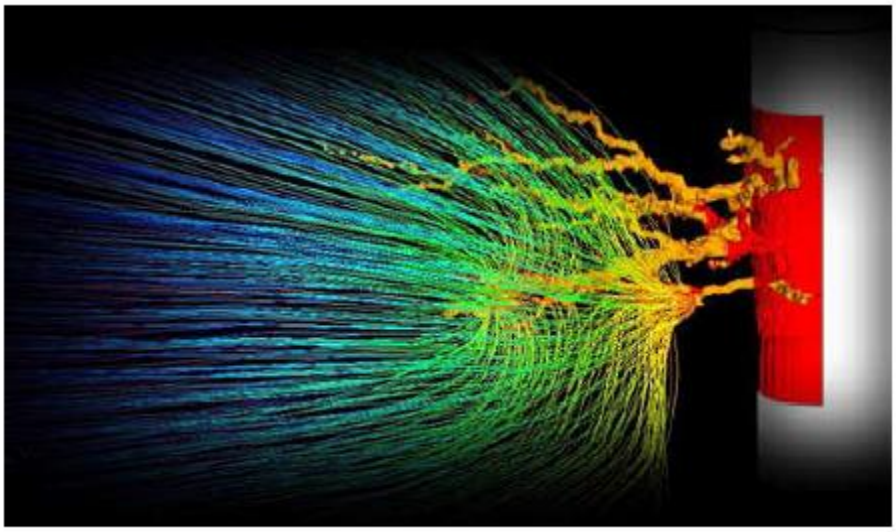

Fig.3. Simulation of wormhole flow characteristics using numerical methods (McDuff *et al.*, 2010)

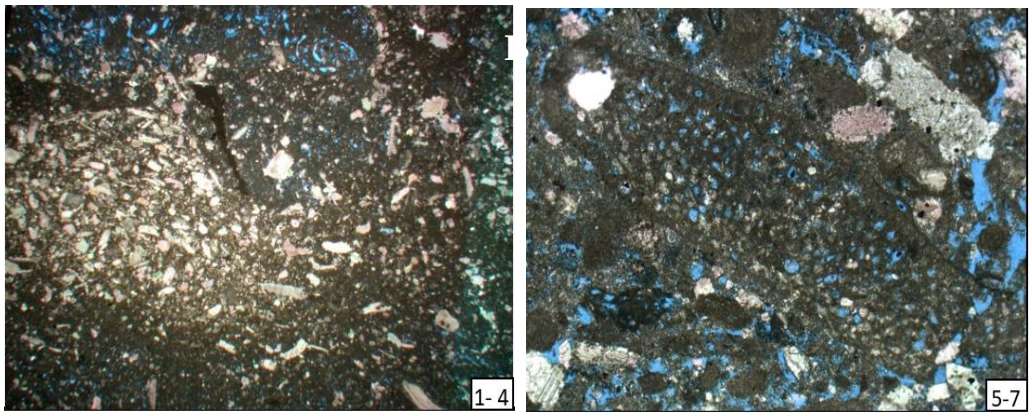

Fig.4. Photomicrographs for the two cored sections of the Mishrif reservoir's well AD-12 **(a)** for samples 1 – 4: a texture with biological burrow texture, the internal ring is composed of echinoderm and core is composed of gastropoda, green algae. The overall texture is an echinoderm, green algae micrite texture and large globogerina formas and beehive worm in amount; (b) for sample 5 – 7: A large amount of grain and concentrated in species. Is predominated by orbitolina debris by strong solution, also named as orbitolina sand grain, visible dividual orbitolina is stored in good shape. Another is echinoderm with a large amount of sand grain with a strong solution and dense gathering

The wireline logging data of Mishrif reservoir's well AD-12 for petrophysical evaluation is provided in Fig. 5. It is necessary to distinguish between oil-rich and oil-poor zones. Resistivity is higher, the oil saturation of these zones is larger than 47 percent, the effective porosity is greater than 15 percent, shale volume of most oil zones is typically less than 10 percent. Mishrif Zone is an oil layer. The effective porosity is around 22 percent, the oil saturation is about 84 percent. We determined the porosity and permeability of 7 rock samples from the Mi4 unit in the Mishrif Formation before chemical treatment. A range of 11 to 24 percent porosity and permeability values of 7.10-15.2 md has been found. The Mishrif reservoir's petrophysical parameters are summarized in Table 1.

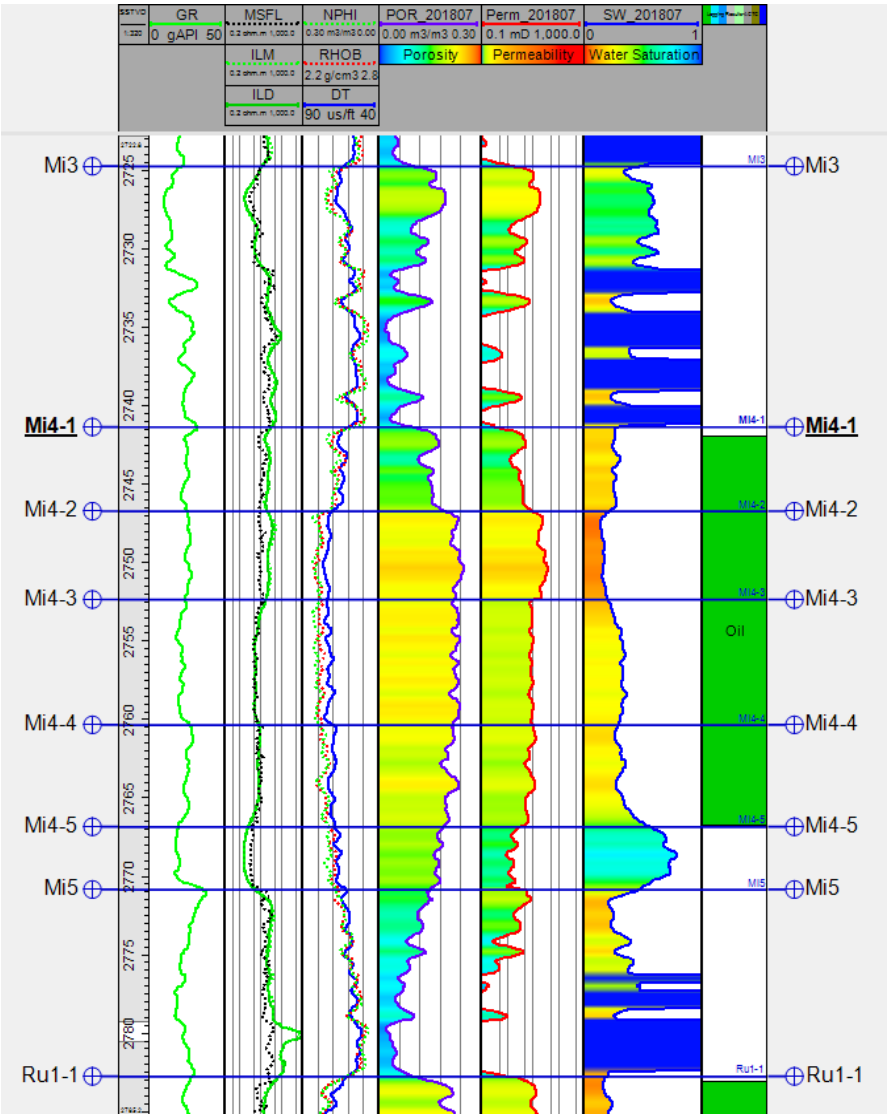

Fig.5. Wireline Logging Interpretation for well AD-12

Table 1. Mishrif Reservoir's Petrophysical Parameters

Well	Formation	Interval (MD)(m)	Thickness (m)	Net_Pay(m)	Avg. POR(%)	PERM (mD)	SW(%)
AD-12	Mi4	2740.1-2765.9	24.8	22.6	19.535	9.748	31.676

2.2. Samples Preparation

The experimental approach is shown in flow chart form in Fig. 6. After coring 7 samples were cut into the required dimensions (2.526cm diameter and a length of 4.571cm each). To prepare the samples for strength tests and core flooding experiments, the ends of the cores were ground to a smooth and parallel surface using end-face grinding. Solvents (toluene and alcohol) were used to clean the core plugs and prepare them for the measurements. Toluene was used to clean any residual oil in the rocks, while alcohol was used to remove precipitated salt within the rock's pores (Isah et al., 2021).

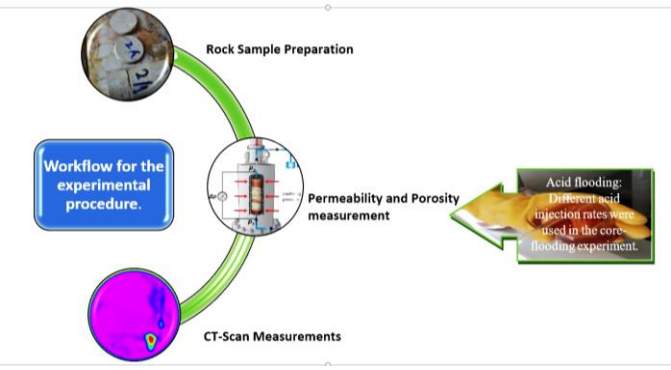

Fig.6. Schematic diagram of the core-flooding system

2.3. Basic Properties of Gelled Acid

Acid diversion is critical for stimulating vertical wells with extended target zones or horizontal wells in carbonates (Bazin, Charbonnel and Onaisi, 1999). Increased viscosity of the injected acid and a delay in the acid interaction with the formation are two benefits of in-situ gelled acids. It improves treatment efficiency. In addition, the gel should break down quickly as the acid is depleted, allowing for better clean-up when the acid treatment is completed (Taylor and Nasr-El-Din, 2001). Table 2 shows the properties of the gelled acid; the viscosity of reacted acid is only 3 mPa.s (equivalent to that of water). Therefore, it can be concluded that there was no harm to the fracture and formation after the acid frac operation.

Table 2. Basic Properties of Gelled Acid

Items	**Test result**
Appearance	Red-brown viscous uniform liquid
Viscosity, 170s^{-1}, 25℃, mPa·s	45
Viscosity, 170s^{-1}, 90℃, 60min, mPa·s	30
Static corrosion rate, 90℃, g/m^2·h	4.79
Surface tension, mN/m	23.75
The capability of stabilizing ferric ion, mg/mL	＞100
The viscosity of reacted acid, mPa.s	3
Chemical's concentration of the diverting acid: 15% HCl, 1.0% ADH-1 (Corrosion inhibitor), 1.5 % ADT-1, and 6% ADZ-1.	

2.4. Core-flooding Experiment

Core flooding tests were conducted for acid injection to establish wormholes in the plugs for each rock sample. Fig. 7 shows a schematic of the core-flooding system. The optimal injection rate was determined after seven acidizing experiments involving varying flow rates. The flow rate ranged from 40 to 400 cc/hr. The core samples were vacuumed with a vacuum pump to ensure complete saturation, and then a brine mainly composed of chloride with a concentration of 15500 ppm-saturated for 2 hours before being left in the desiccator for 48 hours. An ENERPAC pump was used to provide a confining pressure of 2000 psi to the core plugs for all core-flooding experiments. In order to maintain a constant flow with minimal pressure variations, brine was injected first by the ISCO pump. The inlet and outlet pressures at various injection rates were recorded to determine the liquid permeability of the core samples using Darcy's law. Acid was then injected until the wormhole was created which was indicated by a sharp pressure drop. Pressures and injection volumes are monitored and controlled using the core-flooding system's monitoring and control unit.

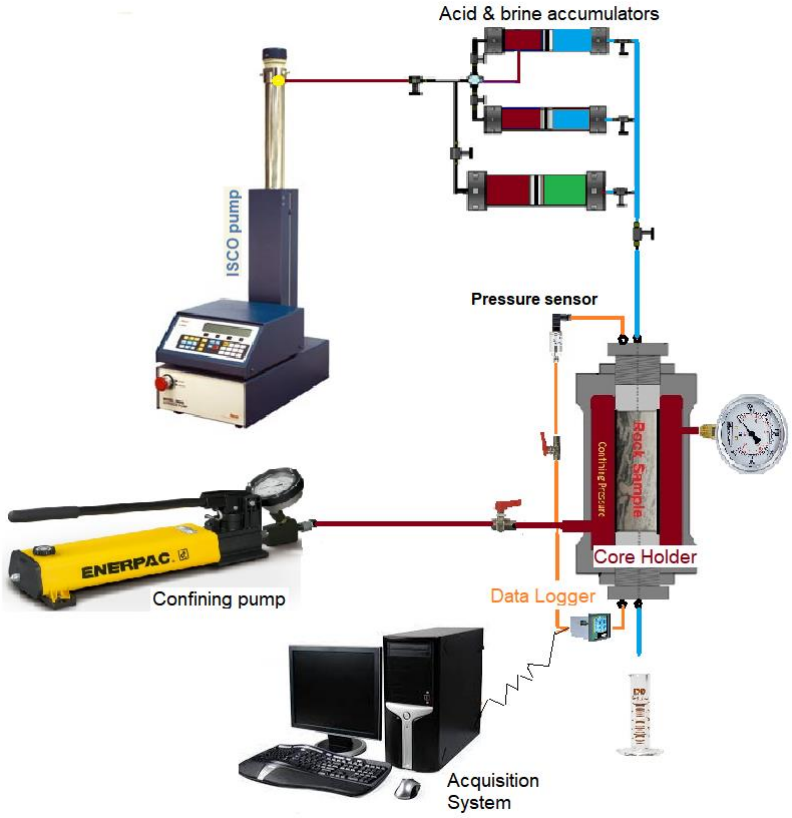

Fig.7. Schematic diagram of the core-flooding system (Alameedy, 2022)

2.5. Porosity and Permeability Measurements

Pre-and post-acidizing core plug porosity and permeability measurements were made. The gravimetric or saturation technique for calculating porosity was employed. The weight of the dry plugs W_{dry}, and the weight of the saturated cores W_{sat}, were used to compute the weight of the saturated brine in the pores of the rock (W_{brine}) given by Equation 1. Pore volume (saturated brine volume) is calculated (Equation 2), where porosity was then computed using Equation 3:

$$W_{brine} = W_{sat} - W_{dry} \quad (1)$$

$$V_p = W_{brine} / \rho_{brine} \quad (2)$$

$$\phi_e = V_p / V_b \quad (3)$$

Permeability was assessed by flowing fluid with a known viscosity through a core sample with known dimensions and then measuring flow rate and pressure drop. In this work, we utilized brine flow through the plug and employed the Darcy law to compute liquid permeability:

$$Q = -\frac{K\,A}{\mu}\frac{\Delta P}{l} \quad (4)$$

where QQ is the instantaneous flow rate (m3s-1), KK is the permeability (µm2), $\mu\mu$ is the dynamic viscosity of brine (Pa.s), $\Delta P\Delta P$ is the pressure drop across the rock plug (Pa), and AA (m2) and ll (m) are the cross-sectional area and length of the core respectively.

2.7. Computed Tomographic (CT) Scanning

CT scanning was used to examine the size and geometry of the wormholes in each rock sample. Helical acquisition 140 kV and 500 mAs resolution CT images were taken to see the micro-scale alterations generated by the chemical interaction between acid solution and the core materials. The mechanical characteristics of various rock types are affected by the size of the wormholes created. As a result, the CT is a valuable instrument for assessing changes in the rock's elastic characteristics.

3. Results

The porosity and permeability were computed before and after the acidizing treatment in order to establish the reasons behind the difficulties encountered during the acid stimulation operation of the Ahdeb oil field, particularly for the development of the Mishrif reservoir. Thus, we systematically analyze the influence of acid treatment on the petrophysical properties of Mi4 formation layer of the Misrif reservoir.

To measure liquid permeability, employ a solution brine at a flow rate of 150 cc/hr and wait till the pressure steadied to 1043 psi (see Fig. 8 a) for plug# 6, then use equation 4 to determine permeability. The differential pressure of Plug #7 is shown in the latter half of Fig. 8 b, where the flow rate was originally set at 150 cc/hr, but as pressure quickly increased owing to the plug's poor permeability, it became essential to lower the flow rate to avoid damaging the pump. Thereby, it was prepared to hold the flow rate of plug#7 at 40 cc/hr while also keeping a steady pressure of 93 psi, leading to the measured permeability of 0.17 md. The porosity of the plug samples before and after acidification is calculated using Equations 1 through 3 in association with the permeability values, as shown in Table 3.

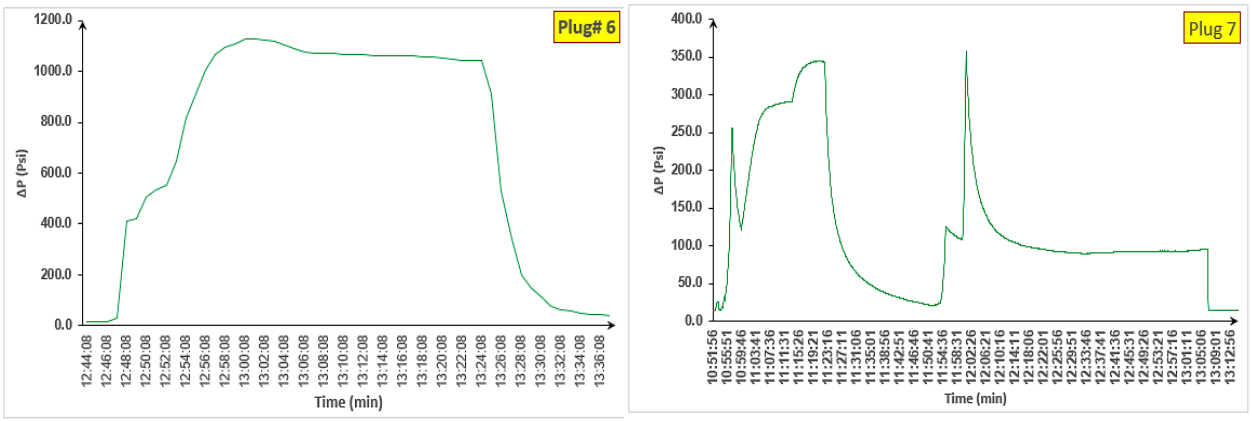

Fig.8. Differential pressure against time, a. Plug#6 flow rate 150 cc/hr , b. Plug#7 flow rate 40 cc/hr

Graphs of differential pressure may also be used to determine whether acid has penetrated the core. Calculations illustrate how long it takes to pump acid into the core as well as how long it takes to produce a wormhole. Remain aware that the term "acid injected" refers to direct acid injection into the core. To reach the core, the acid must pass via tube. Consequently, timing experiments are crucial, as data strongly affect the final outcomes of pore volume to breakthrough. Note that core floods of the actual pressure drop provide a time representation of when a wormhole was created in the preliminary experiment, as shown in Fig. 9, where part A (plug# 6) reached the face of the plug at 11:21 and crossed to the end of the plug at 13:57, indicating the breakthrough occurred; thus, the total time from the core's inlet to outlet is 156 minutes. For plug#7, the time required to reach the core face was 9:15, while the required time to reach the outlet was 13:10, implying a breakthrough time of 235 minutes.

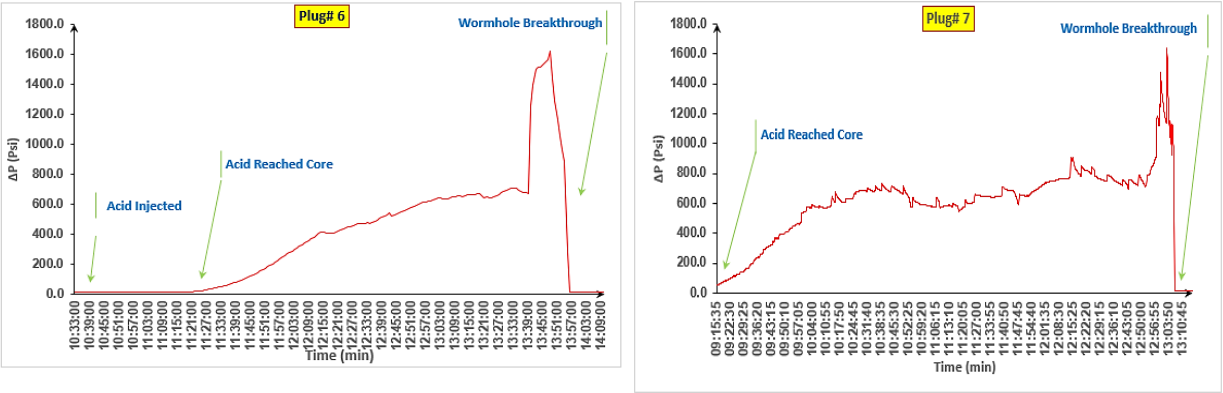

Fig.9. Differential pressure against time acid flooding, (**a)** Plug#6 flow rate 400 cc/hr , **(b)** Plug#7 flow rate 40 cc/hr.

Table 3. Results summary of the petrophysical characteristics tests conducted before and after acidizing.

Plug	Porosity (φ)	Porosity (φ) after acid injection	Permeability (md)	Permeability after acid injection (md)
1	0.15	0.21	0.26	66.5
2	0.10	0.12	0.22	136
3	0.07	0.16	0.06	28.3
6	0.07	0.39	0.37	587
7	0.09	0.27	0.17	38.1
8	0.12	0.25	0.41	323
11	0.13	0.22	0.13	57.9

Acid efficiency curves were constructed using core-flooding tests on core samples (see Fig. 10). Ultimately, the goal is to discover the injection rate that results in the least quantity of acid being used throughout the process (Safari et al., 2014). Typically, the best injection rate results in the optimal possible wormhole, reducing the amount of acid pore volume injection. The reaction rate and convective mass transfer are the factors that regulate the process. Due to face dissolution, substantial amounts of acid are consumed before the wormhole can break through at low injection rates. As a consequence, branching wormholes are formed when the injection rate is substantially greater than the reaction rate. This was corroborated in the work of (Mustafa et al., 2022).

Thus, the development of a wormhole is maximized at a certain Damkohler number (i.e., the ratio of reaction rate to mass transfer). Current rock samples yielded the lowest breakthrough injected pore volume of 3.7 PV at 2.15 cc/min, thus considered optimum injection rate; however, at 0.667 cc/min and 6.67 cc/min, the PVBT are around 24 and 43.5 PV, respectively. The effects of PVBT on the elastic characteristics of the rock samples are shown and analyzed in the subsequent section. The acidizing treatment resulted in a considerable increase in porosity for each of the rock samples. A positive relationship between PVBT and the relative increase in porosity for all rock plugs was observed, as can be seen in Fig. 11. The greater the PVBT, the more likely it is that the relative porosity will grow. This can be attributed to increased rock dissolution/etching as more PV is injected.

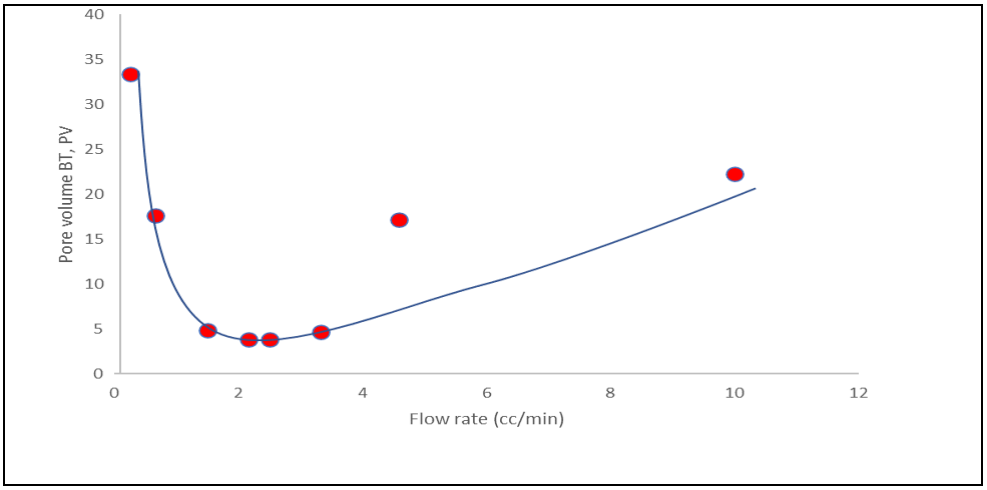

Fig. 10. Pore volume at breakthrough vs. injection rate-- for acidizing experiments

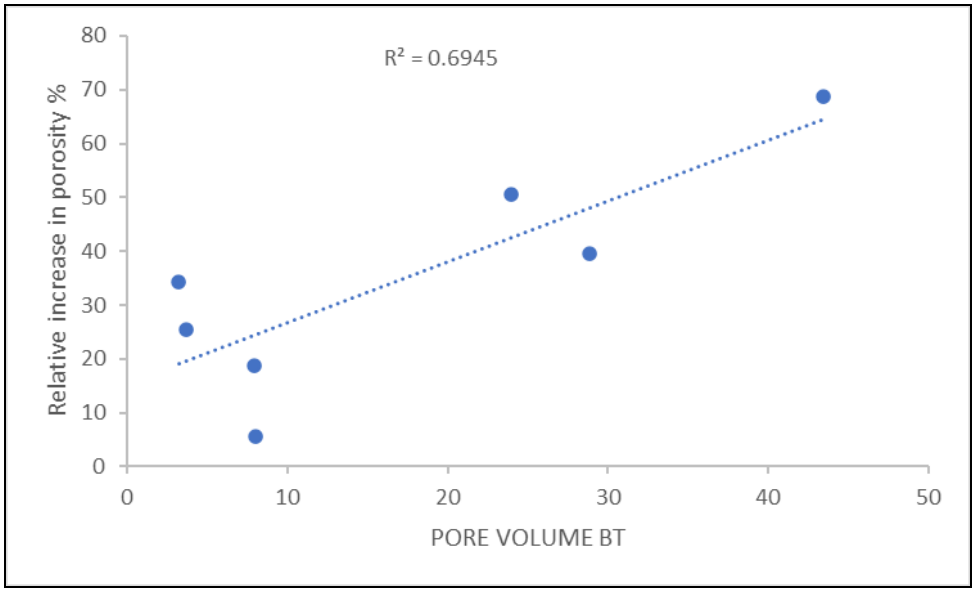

Fig. 11. The effect of PVBT on the improvement of porosity.

Along with the petrophysical analysis, CT scanning was used to visualize the outcome of acid core flooding. It was done using computed tomography, which is non-destructive. Attenuation occurs when X-rays pass through a material. Various injection rates were used on various specimen types in core-flooding testing. Because of this, the wormholes may vary in structure even within the same kind of rock. The rock's mechanical and physical properties may have changed due to the wormhole's size and shape (Zhang, 2015). The 3D Slicer program was used to recreate micro-CT images of two acidized rock samples. Using a medical CT scanner, we scanned the selected plug samples both before and after they were treated with acid. Scanners were tasked with reducing noise and enhancing contrast. Fig. 12 shows CT scans of plug sample No. 6 after acid treatment with a flow rate injection of 400 cc/hr, where the wormhole channel was formed due to convection. After acid treatment at a 40 cm/hr flow rate, four side views of No. 7's face are depicted in Fig. 13, where an acid reaction is a key mechanism that leads to face dissolving (FD).

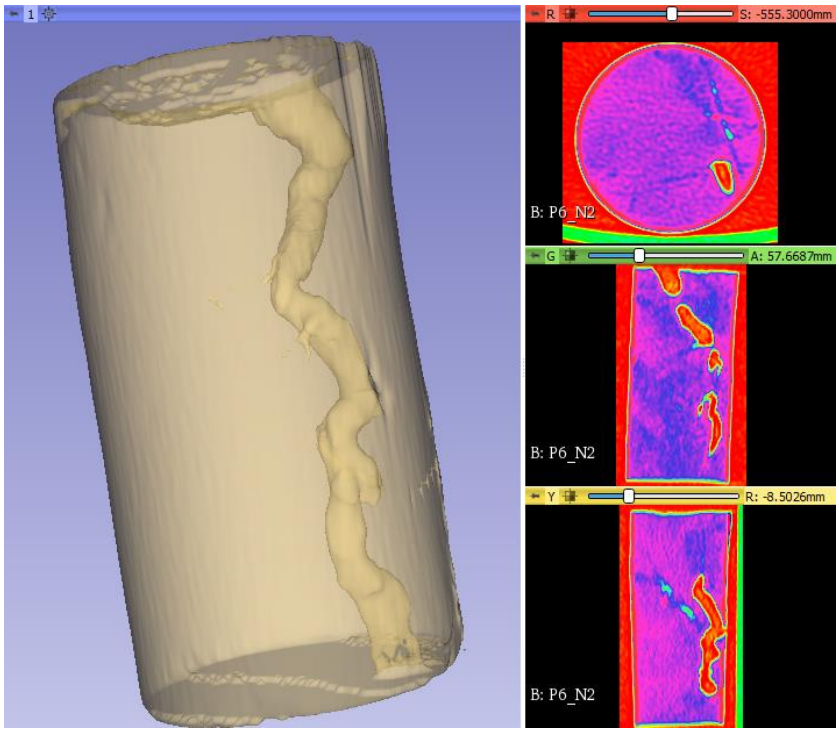

Fig.12. CT images of plug sample No. 6 after acid treatment with a flow rate of 400 cc/hr were obtained.

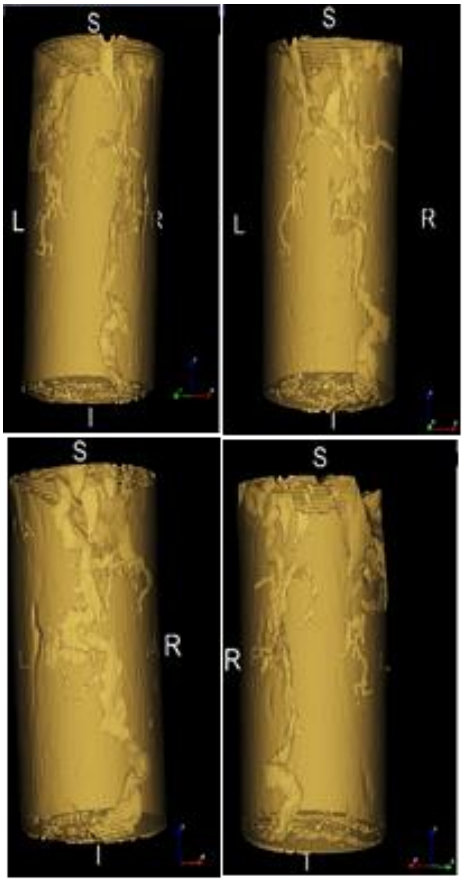

Fig.13. CT-scan, Four side images of No. 7's face were taken after acid treatment at a flow rate of 40 cm/hr.

4. Conclusions

Acid stimulation potentiality in the Mishrif reservoir at the Ahdeb oil field faces significant hurdles, including high injection pressures, with multiple acid treatment failures documented. Oil well stimulation in this deposit has a high failure rate, necessitating more study. Thus, we reported experimental examinations of the petrophysical effects of acidizing on the Misrif reservoir. Acid-flooding tests were conducted on a variety of rock samples to examine the effects of mineralogical variation and ensure that the results were consistent. Porosity and permeability were calculated before and after the acid treatment. The impact of acid-induced wormholes on rock strength was studied and compared to that of naturally occurring rocks.

We discovered that the acid treatment significantly increased the porosity of all the rock samples. All rock plugs showed an increase in porosity due to increased PVBT concentrations. If PVBT is increased, the porosity of the rock will rise, and permeability is likely to increase as a consequence. In order to get the best wormhole and utilize the least amount of acid, the acid efficiency curve showed that 2.15 cc/min injection gave the lowest pore volume injected at a breakthrough of 3.7 PV. After acid treatment, the mechanical characteristics of the rock show signs of deterioration. The CT scan showed that the acid treatment successfully established a channel for oil to move from the reservoir to the wellbore, as expected. Consequently, the wormhole was found to be shorter and more branching at low acid flow rates (0.667 cc/min), indicating that face disintegration occurs and large quantities of acids are consumed before to breakthrough at this rate. The 6.67 cc/min acid injection rate resulted in a larger and longer wormhole. Rock deterioration/sand production/instability is not always the result of acid floods; it relies on other causes. For example, acid-induced fractures and wormholes resulting in increased porosity might be responsible for decreased rock competency. Because of this, separate examinations of the rock mass and the cracked surface strength must be carried out to distinguish between these two factors.

Acknowledgements

The authors are very grateful to the reviewers, Editor in Chief Prof. Dr. Salih M. Awadh, the Secretary of Journal Mr. Samir R. Hijab, and the Technical Editors for their great efforts and valuable comments

References

Alhamad, L., Alrashed, A., Al Munif, E., Miskimins, J., 2020. A Review of Organic Acids Roles in Acidizing Operations for Carbonate and Sandstone Formations, SPE.

Alameedy, U., 2022. Effect of Acid Treatment on The geomechanical properties of rocks: An experimental and numerical investigations in Ahdeb Oil Field, Journal Petroleum Exploration.

Al-Yaseri, A., Abbasi, G.R., Yekeen, N., Al-Shajalee, F., Giwelli, A., Xie, Q., 2022. Effects of cleaning process using toluene and acetone on water-wet-quartz/CO2 and oil-wet-quartz/CO2 wettability. Journal of Petroleum Science and Engineering, 208, 109555.

Bazin, B., 2001. From matrix acidizing to acid fracturing: A laboratory evaluation of acid/rock interactions. SPE Production & Facilities, 16(01), 22-29.

Bazin, B., Charbonnel, P., Onaisi, A., 1999. Strategy Optimization for Matrix Treatments of Horizontal Drains in Carbonate Reservoirs, Use of Self-Gelling Acid Diverter, All Days. SPE.

Cohen, C.E., Ding, D., Quintard, M., Bazin, B., 2008. From pore scale to wellbore scale: Impact of geometry on wormhole growth in carbonate acidization. Chemical Engineering Science, 63(12), 3088-3099.

de Oliveira, T.J., Melo, A.R., Oliveira, J.A., Pereira, A.Z., 2012. Numerical Simulation of the Acidizing Process and PVBT Extraction Methodology Including Porosity/Permeability and Mineralogy Heterogeneity, All Days. SPE.

Fredd, C.N., Fogler, H.S., 1996. Alternative Stimulation Fluids and Their Impact on Carbonate Acidizing, All Days. SPE.

Gdanski, R., 1999. A Fundamentally New Model of Acid Wormholing in Carbonates, All Days. SPE.

Hoefner, M.L., Fogler, H.S., 1988. Pore evolution and channel formation during flow and reaction in porous media. AIChE Journal, 34(1), 45-54.

Hung, K.M., Hill, A.D., Sepehrnoori, K., 1989. A Mechanistic Model of Wormhole Growth in Carbonate Matrix Acidizing and Acid Fracturing. Journal of Petroleum Technology, 41(01), 59-66.

Isah, A., Adebayo, A.R., Mahmoud, M., Babalola, L.O., El-Husseiny, A., 2021. Drainage mechanisms in gas reservoirs with bimodal pores: A core and pore scale study. Journal of Natural Gas Science and Engineering, 86, 103652.

Jardine, D., Wilshart, J.W., 1982. Carbonate Reservoir Description, International Petroleum Exhibition and Technical Symposium. Society of Petroleum Engineers.

Maheshwari, P., Balakotaiah, V., 2013. 3-D Simulation of Carbonate Acidization with HCl: Comparison with Experiments, All Days. SPE.

McDuff, D., Jackson, S., Shuchart, C., Postl, D., 2010. Understanding Wormholes in Carbonates: Unprecedented Experimental Scale and 3D Visualization. Journal of Petroleum Technology, 62(10).

McLeod, H.O., 1984. Matrix Acidizing. Journal of Petroleum Technology, 36(12), 2055-2069.

Mustafa, A., Alzaki, T., Aljawad, M.S., Solling, T., Dvorkin, J., 2022. Impact of acid wormhole on the mechanical properties of chalk, limestone, and dolomite: Experimental and modeling studies. Energy Reports, 8, 605-616.

Panga, M.K.R., Balakotaiah, V., Ziauddin, M., 2002. Modeling, Simulation and Comparison of Models for Wormhole Formation During Matrix Stimulation of Carbonates, All Days. SPE.

Ratnakar, R.R., Kalia, N., Balakotaiah, V., 2012. Carbonate Matrix Acidizing with Gelled Acids: An Experiment-Based Modeling Study, All Days. SPE.

Safari, A., Rashidi, F., Kazemzadeh, E., Hassani, A., 2014. Determining optimum acid injection rate for a carbonate gas reservoir and scaling the result up to the field conditions: A case study. Journal of Natural Gas Science and Engineering, 20, 2-7.

Schechter, R.S., Gidley, J.L., 1969. The change in pore size distribution from surface reactions in porous media. AIChE Journal, 15(3), 339-350.

Taylor, K.C., Nasr-El-Din, H.A., 2001. Laboratory Evaluation of In-Situ Gelled Acids for Carbonate Reservoirs, All Days. SPE.

Zhang, W., 2015. Evaluation of Multi-Stage Acid Fracturing Treatment in Deep Carbonate Formation.